Modeling and Estimation of the Losses of a Multi-Level Inverter with Integrated Battery for Electric Vehicles

Gaël Pongnot, Clément Mayet, Denis Labrousse

▶ **To cite this version:**

Gaël Pongnot, Clément Mayet, Denis Labrousse. Modeling and Estimation of the Losses of a Multi-Level Inverter with Integrated Battery for Electric Vehicles. PCIM Europe 2022, May 2022, Nuremberg, Germany. 10.30420/565822259 . hal-03764921

HAL Id: hal-03764921

https://hal.archives-ouvertes.fr/hal-03764921

Submitted on 30 Aug 2022

HAL is a multi-disciplinary open access archive for the deposit and dissemination of scientific research documents, whether they are published or not. The documents may come from teaching and research institutions in France or abroad, or from public or private research centers.

L'archive ouverte pluridisciplinaire **HAL**, est destinée au dépôt et à la diffusion de documents scientifiques de niveau recherche, publiés ou non, émanant des établissements d'enseignement et de recherche français ou étrangers, des laboratoires publics ou privés.

pcim
EUROPE

Modeling and Estimation of the Losses of a Multi-Level Inverter with Integrated Battery for Electric Vehicles

Gaël Pongnot[1], Clément Mayet[1,2], Denis Labrousse[1,2]

[1] Université Paris-Saclay, ENS Paris-Saclay, CNRS, SATIE, 91190, Gif-sur-Yvette, France
[2] SATIE, UMR 8029, Cnam, F 75003, Paris, France, HESAM Université

Corresponding author: Gaël Pongnot, gael.pongnot@ens-paris-saclay.fr

Abstract

This work is based on an innovative converter structure for an automotive application named Multi-Level Inverter with Integrated Battery. An Energetic Macroscopic Representation of the converter is performed. Conduction and switching losses are evaluated by simulation. The temporal evolution of the electrothermal variables is analyzed. Finally, the efficiency of the converter is calculated as a function of the RMS voltage, the RMS current and the frequency.

1 Introduction

Nowadays, electrification of the automotive powertrain, with technologies such as Battery Electric Vehicles (BEV) or Hybrid Electric Vehicles (HEV), is essential in research and development. The need for energy-saving technologies and greenhouse gas emission reduction is behind this trend. Electromobility arrived on the market at the beginning of the 21st century [1], [2], but is not yet a game-breaker. Further improvements in terms of efficiency, rechargeability, reliability, reconfigurability, compacity, and second life possibility (especially for the battery) are crucial to increase the market penetration of BEV and HEV [3], [4].

The powertrain of conventional BEV uses a battery pack (typically 400 V) composed of a combination of individual battery cells (e.g., 3.3 V Li-ion cells) associated in series and parallel. The reliability of the battery pack is ensured by a Battery Management System (BMS), an additional component that controls the operating conditions of each cell. The battery pack supplies an Electric Machine (EM) using a Voltage Source Inverter (VSI). The VSI uses Pulse Width Modulation (PWM) technique to adapt the DC voltage of the battery to the requested AC voltage. Additionally, an external charger is required to charge the battery.

This typical architecture has many variants due to technical choices or innovative strategies. Variation can occur on converter structure, charging strategy, motor implementation, or even with the combination of batteries with converters [4]–[7].

In previous papers, an architecture using Multi-Level Inverter with Integrated Battery (MLI-IB) has been proposed [8], [9]. The MLI-IB integrates battery cells into cascaded H-Bridge Converters (HBC) and is used to supply the EM of the traction system. It aims to fulfill the roles of VSI, BMS, active cells balancing, charger, and ensuring that each cell is managed individually. Also, the modularity of the MLI-IB offers opportunities for significant reconfigurations and the recovery and reuse of used battery cells, which is a sustainable way of using them considering the current global challenges of energy storage. In addition, different controls can be proposed, especially without using the PWM technique, which can potentially reduce the overall losses of the power electronics devices [9]. Despite the complexity of this topology, the MLI-IB can, therefore, potentially offer significant improvements compared to the conventional topology.

This paper aims to estimate the overall efficiency of the MLI-IB. Two losses sources are considered: conduction and switching in semiconductors switches. The analysis focuses on the power conversion stage without considering battery losses or electromagnetic losses. Modeling are presented using Energetic Macroscopic Representation [10], [11]. Simulations are then performed using MAT-

LAB Simulink.

The proposed architecture is presented in Section 2. Section 3 and Section 4 describe the estimation of conduction and switching losses. Simulation results are provided, and the different sources of loss are compared.

2 Architecture of MLI-IB

Previous papers describe the operation of an MLI-IB system. One of them describes the control [9] while another focuses on the EMR description [8]. This section presents the main principles of this architecture and the associated notations. Figure 1 represents the studied system and defines the variables used in the following equations.

2.1 MLI-IB system principle

The system is composed of three phases. There are M modules per phase. They provide three possible output voltages: $\pm V_{p,m\,\mathrm{bat}}$ and 0. The first index p is the phase index, and the second index m indicates the module index in the phase p. The serial connection of the modules allows obtaining $2M+1$ voltage levels per phase, thus forming a multilevel inverter.

A module consists of a battery and two Unit Conversion Elements (UCE). Each battery is composed of Li-ion cells in series and parallel. The UCEs are MOSFET inverter arms. They provide a current $i_{p,m,n\,\mathrm{out}}$ and a voltage $v_{p,m,n\,\mathrm{out}}$. The index $n \in \{1,2\}$ distinguishes the ECUs of the same module. The association of the two arms creates an H-bridge, which provides the three possible voltage levels at the output of a module. This paper focuses on the study of the losses in the ECUs. The battery behavior will be considered ideal.

2.2 Energetic Macroscopic Representation

Energetic Macroscopic Representation (EMR) is a graphical description tool that describes complex systems [10]. It shows the interactions between elements through action-reaction links and respects systematically the physical causality of a system. This technique highlights the energetic properties of a complex system. It organizes the system into interconnected basic elements: source of energy (green oval), accumulation of energy (orange crossed rectangle), mono (orange square) or

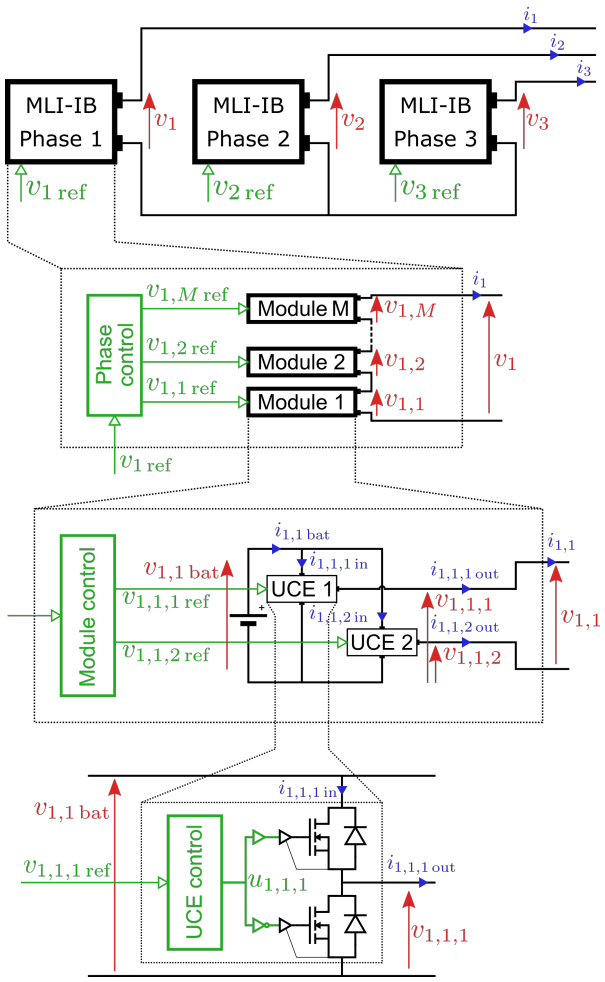

Fig. 1: Structure of a 3-phase MLI-IB

multi (orange circle) domain conversion of energy, and distribution/coupling of energy (double orange square).

In addition, a control can be deduced from the EMR using inversion rules. The control modes are detailed in [9] and are not developed in this paper. The control mode chosen is *direct control*. The reference voltages $v_{p,m,n\,\mathrm{ref}}$ and $v_{p,m\,\mathrm{ref}}$ are deduced from the reference phase voltages v_p according to a control strategy not detailed here.

The EMR of the system (Fig. 2) is developed to perform the simulation in this paper. It is an update of the EMR presented by [8]. The variables of Figure 1 are presented in vector form to have a compact representation. For example, the notation v_p represents a vector of size 3 and $v_{p,m,n\,\mathrm{out}}$ represents a vector of size $6M$.

The study is limited to the converter. Two energy sources are represented: the batteries (BAT) and the electric machine (EM). These sources are con-

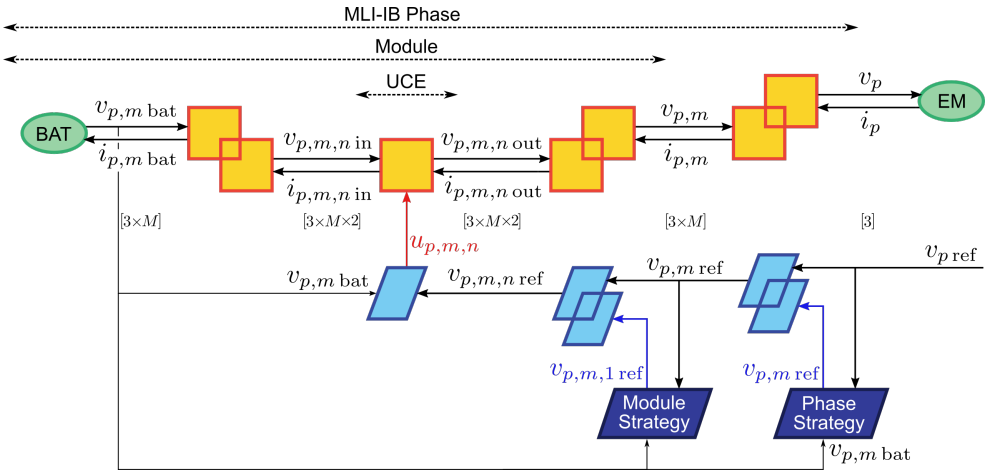

Fig. 2: EMR of a 3-phase MLI-IB without loss

sidered ideal, i.e., the input has no impact on the output of the source. A more realistic behavior can be modeled later by replacing these sources.

2.3 Mathematical description

The EMR is used to organize the model. This subsection presents the different relationships between the variables of the studied system. Theses variables are defined Fig. 1.

2.3.1 Energy sources

The batteries are considered ideal and identical, which leads to Equation (1). The phase current is three-phase sinusoidal (Eq. (2)).

$$v_{p,m\,\mathrm{bat}} = V_{\mathrm{bat}} \tag{1}$$

$$i_p = I_0\sqrt{2}\sin\left(2\pi f t - \frac{2\pi}{3}(p-1)\right) \tag{2}$$

2.3.2 Conversion and coupling elements

Kirchhoff's laws applied to the modules lead to Equations (3) and (4). Applying these laws inside the modules leads to Equations (5) to (8).

$$v_p = \sum_{m=1}^{M} v_{p,m} \tag{3}$$

$$i_{p,m} = i_p \tag{4}$$

$$v_{p,m} = v_{p,m,1\,\mathrm{out}} - v_{p,m,2\,\mathrm{out}} \tag{5}$$

$$i_{p,m,n} = \begin{cases} +i_{p,m} & \text{if } n = 1 \\ -i_{p,m} & \text{if } n = 2 \end{cases} \tag{6}$$

$$v_{p,m,n\,\mathrm{in}} = v_{p,m\,\mathrm{bat}} \tag{7}$$

$$i_{p,m\,\mathrm{bat}} = i_{p,m,1\,\mathrm{in}} + i_{p,m,2\,\mathrm{in}} \tag{8}$$

Equations (9) and (10) reflect the ideal behavior of ECUs. This paper focuses on integrating different sources of losses in these equations.

$$v_{p,m,n\,\mathrm{out}} = u_{p,m,n} v_{p,m,n\,\mathrm{in}} \tag{9}$$

$$i_{p,m,n\,\mathrm{in}} = u_{p,m,n} i_{p,m,n\,\mathrm{out}} \tag{10}$$

3 Conduction losses

In a converter efficiency study, the first losses to consider are conduction losses. They are simple to calculate and generally dominate over the other sources of losses.

3.1 Physical model

A power MOSFET in conduction is traditionally modeled by a resistor $R_{DS_{\mathrm{on}}}$ (Fig. 3). A body diode can also conduct if a significant reverse current is supplied. In practice, it is rarely the case. In particular, the analysis is based on the NVMTS0D4N04C component from ON-semi. For this transistor, the current required for the diode to conduct when the channel is on is greater than the maximum current allowed by the manufacturer. It justifies not considering this diode when the channel is on.

The introduction of this resistance in the model results in a voltage drop proportional to the current between upstream and downstream. This principle

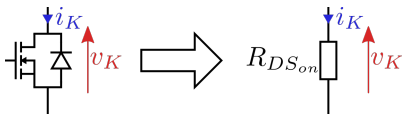

Fig. 3: Model of a MOSFET in conduction

is synthesized in Equation (11). Depending on the state of the system, the output voltage can be decreased or increased compared to the ideal case, see Eq. (5).

$$v_{p,m,n\,\mathrm{out}} = u_{p,m,n} v_{p,m,n\,\mathrm{in}} + (1 - 2u_{p,m,n}) R_{DS_{on}} i_{p,m,n\,\mathrm{out}} \quad (11)$$

This voltage has two effects: the actual voltage is different from the expected voltage, and power is dissipated as heat (losses). Equation (12) gives the expression of the losses. These losses are differentiated between the high-side and low-side transistor, denoted by k, to consider the thermal behavior of each component in future studies.

EMR requires that the product of the action and the reaction, which represent the exchange between two elements, must be the transferred power. A new variable must be introduced to respect this principle. This variable σ is defined by Equation (13). It is homogeneous to a power divided by a temperature and can be interpreted as an entropy transfer.

$$\mathcal{P}_{p,m,n,k\,\mathrm{cd}} = \begin{cases} u_{p,m,n} R_{DS_{on}} i^2_{p,m,n\,\mathrm{out}} & \text{if } k = 1 \\ (1 - u_{p,m,n}) R_{DS_{on}} i^2_{p,m,n\,\mathrm{out}} & \text{if } k = 2 \end{cases} \quad (12)$$

$$\sigma_{p,m,n,k\,\mathrm{cd}} = \frac{\mathcal{P}_{p,m,n,k\,\mathrm{cd}}}{T_{p,m,n,k}} \quad (13)$$

3.2 Energetic Macroscopic Representation

In order to model this behavior, an electrothermal coupling element is introduced in the EMR (Fig. 4). It is placed downstream of the ideal arm. It acts on the output voltage without modifying the current, which corresponds to the model from the previous part. The internal variables defined in Equations (14) and (15) are used to depict the ideal operation.

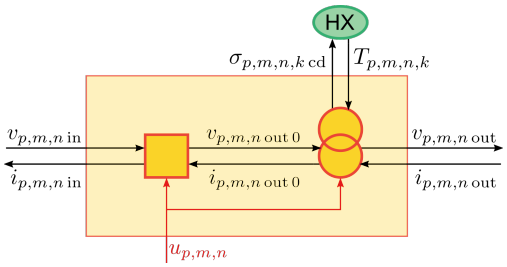

Fig. 4: EMR of an UCE with conduction losses

$$v_{p,m,n\,\mathrm{out}\,0} = u_{p,m,n} v_{p,m,n\,\mathrm{in}} \quad (14)$$

$$i_{p,m,n\,\mathrm{in}} = u_{p,m,n} i_{p,m,n\,\mathrm{out}\,0} \quad (15)$$

A thermal source models an ideal heat exchanger (HX). The heat exchanger imposes a temperature $T_{p,m,n,k} = T_0$ for all transistors. This temperature is used to determine the value of internal parameters of the component, in particular the $R_{DS_{\mathrm{on}}}(T_{p,m,n,k})$.

3.3 Results and discussion

Simulations are performed. Figures 5 and 6 illustrate an operating point (100 V_{RMS}, 100 A_{RMS}, 80 °C, 50 Hz), where voltage and current are considered in phase. Under these conditions $R_{DS_{\mathrm{on}}} = 0.56\,\mathrm{m\Omega}$.

Figure 5 shows the evolution of the electrical variables associated with module 8 of phase 1. The phase voltage v_1 takes the form of a quantified sine, characteristic of the MLI-IB architecture. The voltage $v_{1,8}$ of the module is produced by the difference of the voltages $v_{1,8,1\,\mathrm{out}}$ and $v_{1,8,2\,\mathrm{out}}$ by exploiting the four possible states of the H-bridge: $+V_{\mathrm{bat}}$, $+0$, -0 and $-V_{\mathrm{bat}}$.

The phase current in the ECU produces Joule losses. Whatever the configuration of the module, two transistors are in conduction. Figure 6 represents the losses by conduction in the four switches of module 8 of phase 1. These profiles have to be compared with the output voltages of the ECUs and the phase current. They are characteristic of losses induced by a cut sinusoidal current.

From an overall point of view, the total conduction losses of each phase $\mathcal{P}_{p\,\mathrm{cd}}$ evolve as a double frequency sine with an offset. That is because, whatever the configuration of the modules, $2M$ switches conduct the same phase current. The sum of the

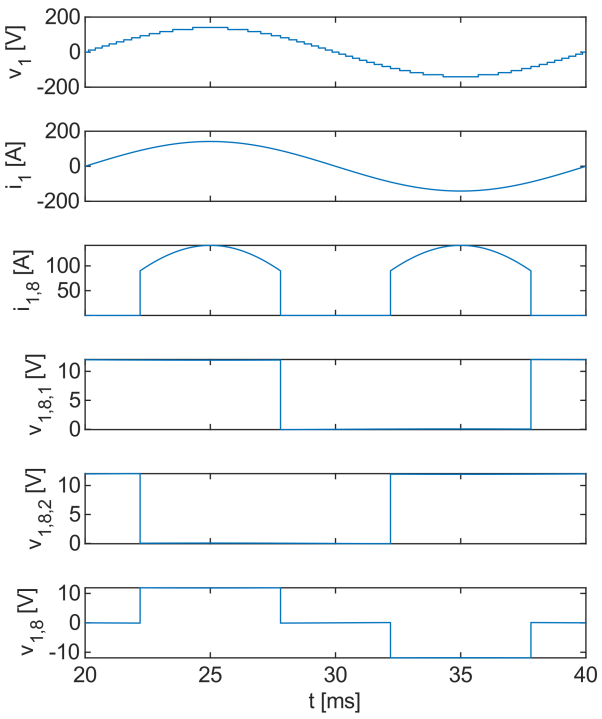

Fig. 5: Evolution of the electrical variables

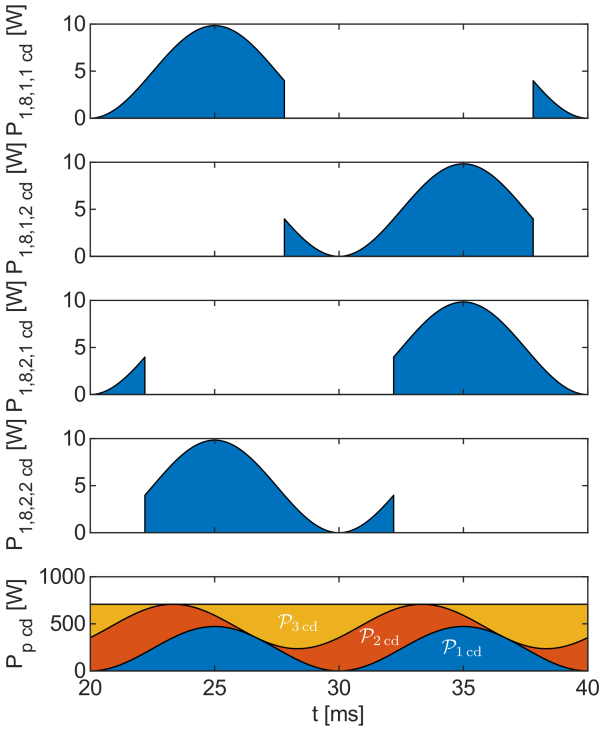

Fig. 6: Conduction losses of a module

conduction losses induced by each phase is constant, which is interesting for the design of the cooling system. Equation (16) gives the expression of the total losses with a unitary power factor. Equation (17) shows that the efficiency increase with the RMS voltage V_0 and decreases with the RMS current I_0. The efficiency will be less suitable for high current at low voltage. From the conduction losses point of view, this behavior is comparable to a classical inverter.

$$\mathcal{P}_{cd} = 6MR_{DS_{\text{on}}}(T_0)I_0^2 \tag{16}$$

$$\eta = \frac{\mathcal{P}}{\mathcal{P}+\mathcal{P}_{cd}} = \frac{1}{1+\frac{2MR_{DS_{\text{on}}}(T_0)I_0}{V_0}} \tag{17}$$

4 Switching losses

The analytical modeling of semiconductors switching is complex. Switching has been studied many times with relative success and several assumptions [12]–[15]. In this paper, the analysis of switching steps is not detailed. The results are based on the following assumptions. The voltage and current variations are linear. The body-diode conducts during the whole dead-time. The reverse recovery energy of the body-diode is linearly dependent on the voltage and does not depend on any other parameter.

4.1 Physical model

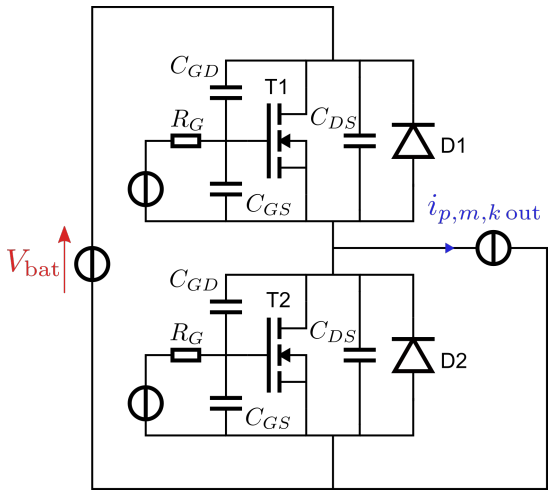

Fig. 7: Dynamic model of a switching arm

Figure 7 presents the dynamic model commonly used when studying switching. This model highlights the parasitic capacitances between the terminals of the MOSFETs. These capacitances are

Tab. 1: Chain of action during switching

Action chain	$I > 0$	$I < 0$
Rising edge	$\mathrm{T}_1 \to \mathrm{D}_2 \to \mathrm{T}_2$	$\mathrm{T}_1 \to \mathrm{D}_1 \to \mathrm{T}_2$
Falling edge	$\mathrm{T}_2 \to \mathrm{D}_2 \to \mathrm{T}_1$	$\mathrm{T}_2 \to \mathrm{D}_1 \to \mathrm{T}_1$

Tab. 2: Energy lost in the channel

$\mathcal{E}_C$	$I > 0$	$I < 0$
Rising edge	$\frac{V_{\mathrm{bat}} I}{2}(t_{a2} + t_{b2})$	$-\frac{V_{\mathrm{bat}} I}{2}(t_{a1} + t_{b1})$
Falling edge	$\frac{V_{\mathrm{bat}} I}{2}(t_{a1} + t_{b1})$	$-\frac{V_{\mathrm{bat}} I}{2}(t_{a2} + t_{b2})$

non-linear, in particular $C_{GD} = C_{RSS}$, which is why the curves $C_{RSS}(V_{DS})$ and $V_{GS}(Q_G)$ provided by the manufacturer are useful.

Switching takes place in different stages depending on the control signal (rising edge or falling edge) and the current direction. In order to avoid short circuits, a dead time of duration t_m is set up. During this dead time, the body-diode of the corresponding transistor conducts. Table 1 summarizes the steps between the conducting elements.

The losses are of three kinds: losses in the transistor channel, conduction losses in the body-diode, and reverse recovery losses in the body-diode [12]. The losses in the channel for a current $I = i_{p,m,k\,\mathrm{out}} > 0$ are located in the transistor T1. If the current is negative, they are located in the transistor T2. The conduction losses of the body-diode are located in D2 for a direct current and inversely. The reverse recovery losses occur only for a rising edge with a direct current (D2) or a falling edge with an inverse current (D1). Since transistors and body-diodes cannot be physically distinguished, the losses of T1 and D1 are grouped, idem for T2 and D2.

4.1.1 Channel losses

A study of the voltage-current product of the transistor and its transient regime is necessary to quantify the losses in the channel. This study considers two stages where either the voltage or the current evolves linearly. Then, the duration of these two stages must be determined by solving the dynamic equations of the circuit. Table 2 presents the energies lost in the channel depending on the durations defined in Equations (18) to (21).

$$t_{a1} = \frac{Q_{GD}(V_{\mathrm{bat}}) R_G}{V_T + \frac{|I|}{g_{FS}} - V_{GL}} \tag{18}$$

$$t_{b1} = \tau \ln\left(1 + \frac{|I|}{g_{FS}(V_T - V_{GL})}\right) \tag{19}$$

$$t_{a2} = \tau \ln \frac{1}{1 - \frac{|I|}{g_{FS}(V_{GH} - V_T)}} \tag{20}$$

$$t_{b2} = \frac{Q_{GD}(V_{\mathrm{bat}}) R_G}{V_{GH} - \frac{|I|}{g_{FS}} - V_T} \tag{21}$$

The voltages V_{GH} and V_{GL} correspond to the high and low levels of the gate control voltage. The transconductance g_{FS} is considered constant, as is the gate threshold voltage V_T. The characteristic time is set to $\tau = R_G C_{ISS}$ with the gate resistance R_G and the input capacitance $C_{ISS} = C_{GS} + C_{GD}$ considered constant. The Gate-to-Drain charge Q_{GD} varies according to Equation (22), with the reverse transfer capacitance $C_{RSS}(V_{DS})$ taken from the manufacturer's datasheet.

$$Q_{GD}(V_{DS}) = C_{RSS}(V_{DS}) \times \left(V_{DS} - V_T - \frac{|I|}{g_{FS}}\right) \tag{22}$$

4.1.2 Conduction losses in body-diode

The conduction losses of the body-diodes depend directly on the dead-time t_d chosen. For simplicity, the body-diode is considered conductive during the whole dead-time. The energy $\mathcal{E}_{\mathcal{D}}$ dissipated by the diode during this period is expressed by the Equation (23). This energy is the same whatever the conducting diode.

$$\mathcal{E}_D = (V_F |I| + R_D I^2) t_d \tag{23}$$

4.1.3 Reverse recovery losses in body-diode

When there is recovery, the energy dissipated by this phenomenon can be expressed by the Equation (24). The Reverse Recovery Charge Q_{RR} is considered to be constant, so this energy is independent of the output quantities of the system.

$$\mathcal{E}_{\mathrm{rec}} = Q_{RR} V_{bat} \tag{24}$$

4.2 Energetic Macroscopic Representation

Unlike conduction losses, the integration of switching losses in EMR is unclear. These losses do not result in a drop in output voltage or an increase in input current, but rather both at the same time, mixed with an overlap between the output voltage and the input current. Therefore, several modeling choices are possible: replace the ideal conversion element (orange square) with an electrothermal coupling element, consider these losses as a pure voltage drop or a pure current increase, or any other consistent idea. This study considers the increase of the input current, as shown in Figure 8. An electrothermal coupling block is inserted upstream of the ideal converter. Then a coupling element is necessary for the parallel thermal loss sources.

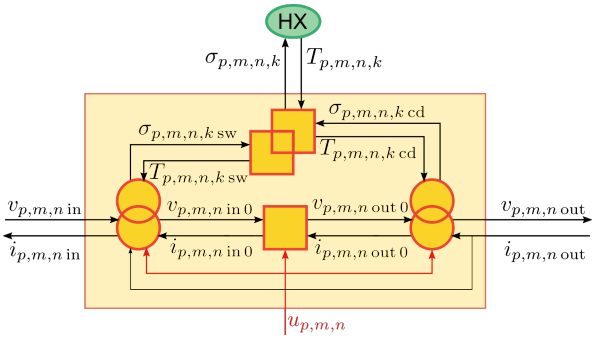

Fig. 8: EMR of an UCE with conduction and switching losses

In order to stay close to the physical waveform, edge detection of the control signal is considered. At the edges, the energies to be dissipated are calculated and transformed into additional current applied during a calculated time. For example, in the case of a positive current rising edge, an additional current $\frac{1}{2} i_{p,m,n\,\mathrm{out}}$ is applied during a time $t_{a2} + t_{b2}$. The power $\mathcal{P}_{p,m,n,k\,\mathrm{sw}}$ is the result of the calculated energy divided by the time of application of the corresponding current, applied to the component during the dissipative period.

4.3 Results and discussion

Simulations using the presented model are performed. Figure 9 presents the temporal evolution of the variables for a particular operating point (100 V_{RMS}, 100 A_{RMS}, 80 °C, 1000 Hz). The previous choices lead to a current peak at the start of conduction and a progressive decrease during blocking. This behavior is not an exact representation of reality, but it allows to estimate the losses and to locate them correctly over time.

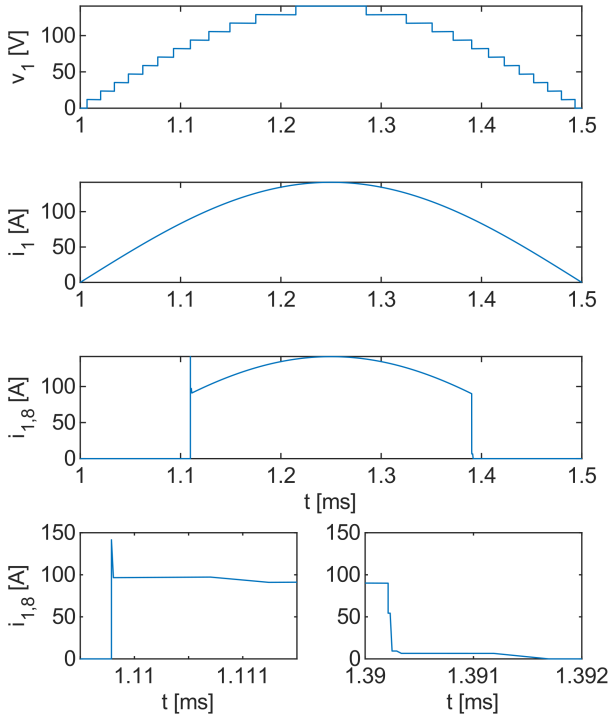

Fig. 9: Temporal evolution of electrical quantities

Equations (23) and (24) and table 2 express the energies dissipated by the phenomena taking place during switching. Therefore, the power dissipated by the switching is proportional to the frequency. Figure 10 shows the switching losses as a function of the RMS current I_0 and the RMS voltage V_0 for two typical operating frequencies. As a first approximation, we can consider that these losses vary as $V_0 I_0$. The proportionality with frequency is also verified.

The magnitudes involved in conduction and switching are not the same. Switching losses are almost negligible and have little influence on the total losses (less than a few percent). The ratio between switching losses and conduction losses is maximum when current is low and voltage is high but stays under 3% for 15 A.

Figure 11 shows the evolution of the efficiency as a function of V_0 and I_0 for the two typical frequencies. The curve presented corresponds to Equation (17), and the influence of the frequency is not perceptible, which shows once again that the switching losses have little influence on the total losses. However,

a study with more simulation points will have to be conducted to see the influence of the number of activated modules on the losses.

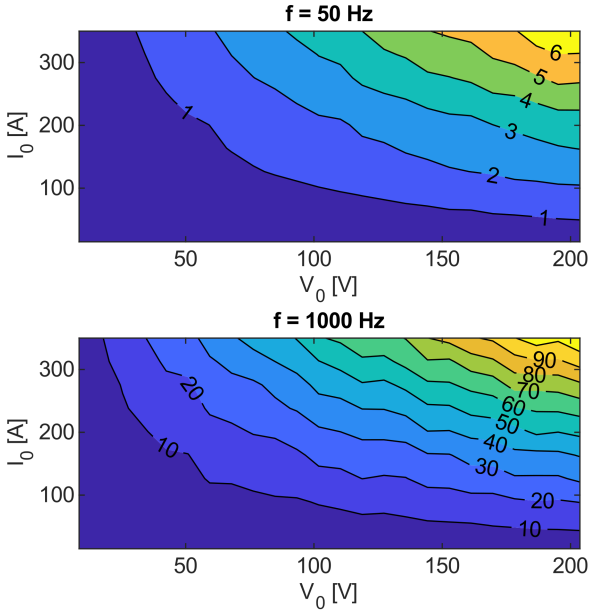

Fig. 10: Switching losses map [W]

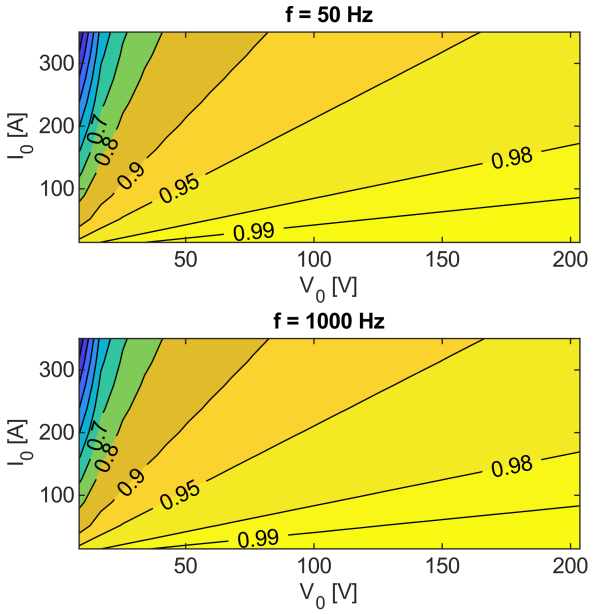

Fig. 11: Efficiency with conduction and switching losses

5 Conclusion

The modeling studied aims to estimate the efficiency of an innovative Multi-Level Inverter with an Integrated Battery. Therefore, it requires the consideration of conduction and commutation losses. The modeling shown in this paper is conducted using a recent technique: Energetic Macroscopic Representation, which insists on causality and power transfer.

This work highlights that an architecture MLI-IB can have benefits despite increasing the number of switches. Indeed, this structure has constant conduction losses and negligible switching losses. The extraction of information for each component and the multiscale modeling is allowed by EMR.

However, switching losses modeling suffers from an insufficient representativity of the temporal evolution of its electrical variables. Improvements must be made on the switching modeling, even if this paper shows them lower than conduction losses. Further studies will study the evolution of the efficiency with more details, mainly to show the influence of the number of activated modules on switching losses. Other aspects of the entire system should be considered in future work, like batteries, traction chain, heat exchange, or temperature dependence of physical parameters. A long-term research axis is to model the complete system on different operating cycles. Performance maps will be helpful to achieve this goal.

6 Acknowledgments

This paper has been achieved within IBIS project, which is funded by ADEME (*Agence de l'environnement et de la maîtrise de l'énergie*) through "Le Programme d'investissements d'avenir (PIA)".

References

[1] B. Frieske, M. Kloetzke, and F. Mauser, "Trends in vehicle concept and key technology development for hybrid and battery electric vehicles," in *2013 World Electric Vehicle Symposium and Exhibition (EVS27)*, Nov. 2013, pp. 1–12. DOI: 10.1109/EVS.2013.6914783.

[2] C. Chan, "Overview of Electric, Hybrid, and Fuel Cell Vehicles," in *Encyclopedia of Automotive Engineering*, John Wiley & Sons, Ltd, 2014, pp. 1–14. DOI: 10.1002/9781118354179.auto061.

[3] B. Sarlioglu, C. T. Morris, D. Han, and S. Li, "Benchmarking of electric and hybrid vehicle electric machines, power electronics, and batteries," in *2015 Intl Aegean Conference on Electrical Machines Power Electronics (ACEMP), 2015 Intl Conference on Optimization of Electrical Electronic Equipment (OPTIM) 2015 Intl Symposium on Advanced Electromechanical Motion Systems (ELECTROMOTION)*, Sep. 2015, pp. 519–526. DOI: 10.1109/OPTIM.2015.7426993.

[4] M. Ehsani, K. V. Singh, H. O. Bansal, and R. T. Mehrjardi, "State of the Art and Trends in Electric and Hybrid Electric Vehicles," *Proceedings of the IEEE*, vol. 109, no. 6, pp. 967–984, Jun. 2021. DOI: 10.1109/JPROC.2021.3072788.

[5] M. Ehsani, Y. Gao, S. Longo, and K. M. Ebrahimi, *Modern Electric, Hybrid Electric, and Fuel Cell Vehicles*, Third. Boca Raton: CRC Press, Mar. 2018. DOI: 10.1201/9780429504884.

[6] J. Channegowda, V. K. Pathipati, and S. S. Williamson, "Comprehensive review and comparison of DC fast charging converter topologies: Improving electric vehicle plug-to-wheels efficiency," in *2015 IEEE 24th International Symposium on Industrial Electronics (ISIE)*, Jun. 2015, pp. 263–268. DOI: 10.1109/ISIE.2015.7281479.

[7] L. Komsiyska, T. Buchberger, S. Diehl, M. Ehrensberger, C. Hanzl, *et al.*, "Critical Review of Intelligent Battery Systems: Challenges, Implementation, and Potential for Electric Vehicles," *Energies*, vol. 14, no. 18, p. 5989, Jan. 2021. DOI: 10.3390/en14185989.

[8] C. Mayet, D. Labrousse, R. Bkekri, F. Roy, and G. Pongnot, "Energetic Macroscopic Representation and Inversion-Based Control of a Multi-Level Inverter with Integrated Battery for Electric Vehicles," in *2021 IEEE Vehicle Power and Propulsion Conference (VPPC)*, Gijon, Spain: IEEE, Oct. 2021, pp. 1–6. DOI: 10.1109/VPPC53923.2021.9699228.

[9] C. Mayet, D. Labrousse, A. Dittrick, B. Revol, R. Bkekri, and F. Roy, "Simulation and Control of a New Integrated Battery System for Automotive Applications," in *PCIM Europe Digital Days 2021; International Exhibition and Conference for Power Electronics, Intelligent Motion, Renewable Energy and Energy Management*, May 2021, pp. 1–6.

[10] A. Bouscayrol, J.-P. Hautier, and B. Lemaire-Semail, "Graphic Formalisms for the Control of Multi-Physical Energetic Systems: COG and EMR," in *Systemic Design Methodologies for Electrical Energy Systems*, John Wiley & Sons, Ltd, 2012, ch. 3, pp. 89–124. DOI: 10.1002/9781118569863.ch3.

[11] H. Yu, R. Lu, T. Wang, and C. Zhu, "Energetic Macroscopic Representation based modeling and control for battery/ultra-capacitor hybrid energy strorage system in HEV," in *2009 IEEE Vehicle Power and Propulsion Conference*, Sep. 2009, pp. 1390–1394. DOI: 10.1109/VPPC.2009.5289452.

[12] D. A. Grant and J. Gowar, *Power Metal-Oxide Semiconductor Field Effect Transistors: Theory and Applications*. Wiley & Sons, Incorporated, John, 1989.

[13] J. Lutz, H. Schlangenotto, U. Scheuermann, and R. De Doncker, "MOS Transistors," in *Semiconductor Power Devices: Physics, Characteristics, Reliability*, J. Lutz, H. Schlangenotto, U. Scheuermann, and R. De Doncker, Eds., Berlin, Heidelberg: Springer, 2011, pp. 283–314. DOI: 10.1007/978-3-642-11125-9_9.

[14] H. Raee, A. Rabiei, and T. Thirnger, "Analytical prediction of switching losses in MOSFETs for variable drain-source voltage and current applications," in *2013 IEEE 8th Conference on Industrial Electronics and Applications (ICIEA)*, Jun. 2013, pp. 705–709. DOI: 10.1109/ICIEA.2013.6566458.

[15] S. Eskandari, K. Peng, B. Tian, and E. Santi, "Accurate Analytical Switching Loss Model for High Voltage SiC MOSFETs Includes Parasitics and Body Diode Reverse Recovery Effects," in *2018 IEEE Energy Conversion Congress and Exposition (ECCE)*, Sep. 2018, pp. 1867–1874. DOI: 10.1109/ECCE.2018.8557515.